# Experimental study and numerical optimization of tensegrity domes – A case study

Karol Winkelmann, Filip Kłos, and Mateusz Rąpca

View Online  Export Citation

## ARTICLES YOU MAY BE INTERESTED IN

# Experimental Study and Numerical Optimization of Tensegrity Domes – a Case Study

## Karol Winkelmann[1, a)], Filip Kłos[1] and Mateusz Rąpca[1]

[1]*Gdańsk University of Technology, Faculty of Civil and Environmental Engineering, Narutowicza Street 11/12, 80-213 Gdańsk, Poland*

a)Corresponding author: karolwin@pg.gda.pl

**Abstract.** The paper deals with the design, experimental analysis and numerical optimization of tensegrity dome models. Two structures are analyzed – a Geiger system dome (preliminary dome), with PVC-U bars and PA6/PP/PET tendons and a Fuller system dome (target dome), with wooden bars and steel cables as tendons. All used materials are experimentally tested in terms of Young's modulus and yield stress values, the compressed bars are also tested for the limit length demarcating the elastic buckling from plastic failure. The data obtained in experiments is then implemented in SOFiSTiK commercial software FE model. The model's geometrical parameters are considered uniform random variables. Geometrically and materially nonlinear analysis is carried out. Based on the obtained structural response (displacements), a Monte Carlo simulation – based approach is incorporated for both structural design point formulation and the SLS requirements fulfillment analysis. Finally, an attempt is made to erect the Fuller dome model in order to compare the numerical results of an experimentally–derived model with the in situ measurements of an actual structure.

## TENSEGRITY STRUCTURES – INTRODUCTION

Tensegrity structures were proposed by Richard Buckminster Fuller and Kenneth Snelson in early 1950's. The term "tensegrity" is a portmanteau of "tensional integrity", which highlights their main feature – the internal stabilization of the elements loaded with pure axial forces only – tension (tendons) or compression (bars). This means the structure fails only if the tendons yield or the bars buckle.

In modern engineering, tensegrity structures are mostly used in aerospace and civil engineering. Their interesting architectural form is one of its basic and main advantages. The other advantages of this type of structures lie in their good load–to–weight ratio (which enables the possibility of roofing a large area using only a small amount of materials, hence gaining a lightweight and slender structure) and a clear separation of elements in terms of transmitted internal forces (which significantly simplifies the design phase of such structures) [1].

## GEOMETRY OF CONSTRUCTED DOMES AND MATERIALS USED

Two tensegrity domes were designed – both suspended on a wooden octagonal tholobate support of a 6.25 m diameter. The first structure was a Geiger system dome, the latter – a Fuller system dome. Illustrative sketches of spatial layout of these typical solutions are shown in Fig. 1a and Fig. 1b respectively, the natural scale concept is also enclosed in Fig. 1c.

The top view of the Geiger's dome shows a system similar to a spider's web structure – centrally converging lines (bar – tendon girders) are interconnected by clasping tendons (two coplanar elements). In turn, the top view of the Fuller's dome can be characterized by triangular fields, with only one clasping tendon at time, connected only to the bottoms of adjacent bars. This type of arrangement of components increases the global stiffness and the stability of the system, compared to the Geiger's approach, it also shows a much greater torsional stiffness. On the other hand, it's assembly is perceived as much more complicated, requiring a multi–phase realization [2].

Importantly, tensegrity systems are flexible and highly prone to large deformations. Due to this susceptibility, an analysis which takes into account the geometry update along with subsequent load increments, is needed. A typical approach is to use the geometrically nonlinear structural analysis (GNA) in a load–control variant [3].
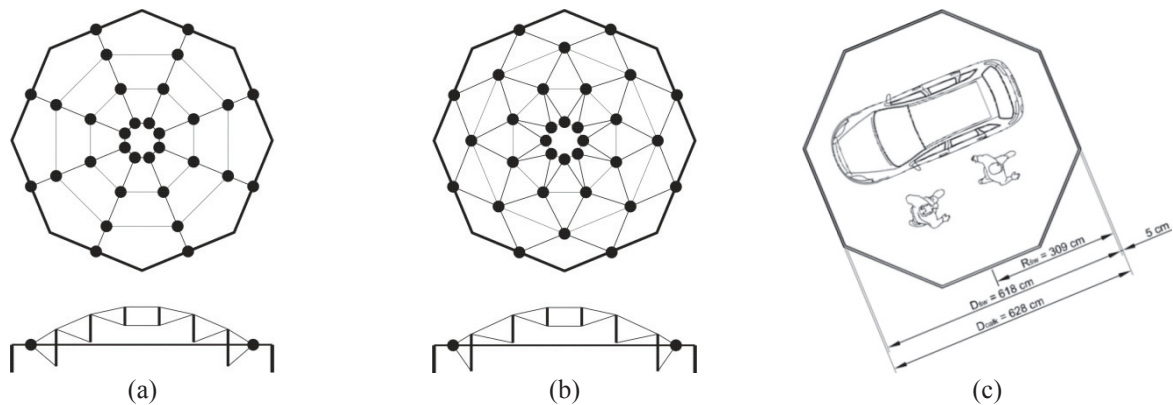


**FIGURE 1.** Illustrative sketches of spatial layout of tensegrity systems considered in the work: a Geiger system dome (a), a Fuller system dome (b) and the natural scale concept (c)

In the first case (Geiger dome) the bars were made of PVC–U pipes, while the tendons were made of nylon technical line (PA6/PP/PET monofilament). Synthetics, alongside composites, are rarely used in construction as load–bearing elements, hence their suitability for structural design required primary experimental tests [4].

The results acquired during those experiments were not only satisfactory, but the observation of the non–classic material behaviour successfully became the basis for the optimization procedures and resolving technical difficulties encountered during the preliminary tests helped shape the final form of nodes applied to the real–life structure.

In the second case (Fuller dome) the bars were made of structural timber (pine) cylinders and the tendons were made of S30400 stainless steel cables.

## EXPERIMENTAL STUDY OF APPLIED MATERIALS

The experimental tests of the materials applied in the study were conducted on the Zwick/Roell Z 400 testing machine, fulfilling the respective PN–EN–ISO standards guidelines on performing strength tests of steel, timber and plastics. For each of the material, 10 – 20 batches of samples, 10 samples each, were tested.

For bar elements, a static compression tests for Young's modulus and buckling tests, meant to assess the critical force of the elements, were performed. For the latter purpose, the samples were examined assuming a variation in their length, in order to obtain the limit length of the bar demarcating the elastic buckling from plastic failure.

For tendons, static tensile tests for Young's modulus, in two variants were carried out. At first, the materials were put in the clamps of the testing machine directly, however the construction method of the real – life nodes forced to analyze the samples also with snap hooks or thimbles attached. A yield stress value was assessed – it was observed as similar in case of direct and indirect anchoring. Also, the rupture force of joints was calculated. It is worth noting, that for every element, the failure mechanism was observed to discern samples providing probably faulty results due to the appearance of imperfections during the test, caused by undesired phenomena regarding the material.

The Young's moduli were calculated in MagicPlot software, as the tangent to the uniaxial test normal stress versus the longitudinal strain graph, in the middle part of its linear path.

The elastic moduli are presented in the paper as a mean value of chosen observations, omitting the values from clearly faulty samples (i.e. when a cable untangled, a joint split or a snap hook failed). Whereas steel and plastics were considered in the tests as isotropic, the timber was strongly anisotropic. However, the samples were prepared in such a way, that the rings of the timber were always perpendicular to the sample's longitudinal axis. This way, an longitudinal Young's modulus ($E_L$) was guaranteed to be assessed, and the other moduli were assessed as $E_R = 0.1\ E_L$ and $E_T = 0.05\ E_L$, respectively, according to [5]. The Poisson's ratios were not assessed, they were taken from literature depending on the material itself and the obtained values for its elastic modulus.

The results of the studies were used in the formulation of the numerical model used for parametric analysis.

# Compressed elements' experimental tests

The PVC–U elements had a tubular cross–section, with an inner diameter of $d_i = 17.46$ cm, and an outer diameter of $d_o = 21.34$ cm. Wooden elements had a full circular cross–section with a diameter of $d = 16.70$ cm.

The bar members were at first subjected to a static compression test. During the test, proper placement of the samples was strictly required. For this purpose, the elements were pre–loaded with a 5 N starting force, so that sufficient frictional forces were created between the sample and the pressure plates to ensure that the sample was properly positioned. The force was applied by a traverse in a displacement control approach, the test was carried out with a constant speed of 15 mm/min.

Both rigid and pinned supports (for the purpose of slender samples compression) were considered for the samples. Obtaining the freedom of rotation at the ends of the samples proved somewhat problematic. For the plastic tubes, the issue was solved by indirect supporting – a short bolt with a spherically shaped head was inserted into the ends of the tubes. The pine timber samples were polished in such a way, that their ends formed a spherical shape.

The test stands for each compressed specimen are shown in Fig. 2a and Fig. 2b. Please note, that the photo is taken after an experiment – both slender elements shown a buckling–induced plastic (brittle, for timber) failure.



(a)          (b)

**FIGURE 2.** The test stand for compressive tests – a pinned support scheme for both PVC–U elements, where a bolt was used (a) and for timber elements, with a spherical ending formed by polishing (b) – photo taken after a buckling–induced plastic failure
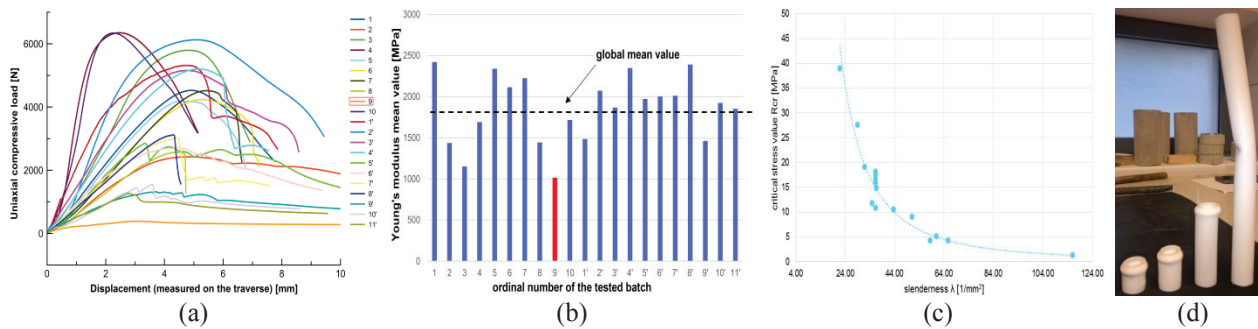


(a)      (b)      (c)      (d)

**FIGURE 3.** Results of uniaxial compression test of PVC–U elements: load – displacement diagrams of representative samples for 20 batches used (a), mean values of Young's modulus for every batch (b), the dependence between the slenderness and the critical stress value for samples tested for buckling occurrence (c) and a photo showing different plastic failure modes (d)

For each PVC–U sample, specific load – displacement diagrams were obtained based on the results provided by the testing machine. A representative sample from each batch was demarcated in Fig. 3a. Please note, that for a clearly faulty batch no 9, a substitute batch no 11' was introduced. The *prim* symbol demarcates samples tested in different days. The uniaxial test results shown in Fig. 3a were recalculated into a $\sigma/\varepsilon$ relationship, and further – into respective elastic moduli in MagicPlot, as previously indicated. The mean values of the modulus for each batch are shown in Fig. 3b, along with a dashed line indicating a global mean value of Young's modulus of PVC–U assessed on the basis of the experiment. The mean value of Young's modulus was calculated equal to $E_{mean} = 1851.947$ MPa (ca. 13% lesser than the minimal reference value for PVC–U equal to $E_{PCV–U} = 2140$ MPa [6]), the obtained standard deviation of the modulus was equal to $s_E = 415.529$ MPa, which gives a variance coefficient $CoV = 0.22$, strongly exceeding the value of 0.05, acceptable for structural materials' tests [6].

Furthermore, a test using 20 PVC–U samples with various lengths was conducted to assess the length demarcating the plastic failure and the elastic buckling – the minimal length of the sample for which the buckling was observed was 150 mm. In Fig. 3c the dependence between the slenderness and the critical stress value was shown, and an Eulerian hyperbola was approximated. Please note, that only the results from buckled samples were taken into account, the samples which failed in a plastic manner were omitted. A post – failure illustration of samples with different lengths is shown in Fig. 3d, the rightmost sample failed by buckling – induced mechanism.
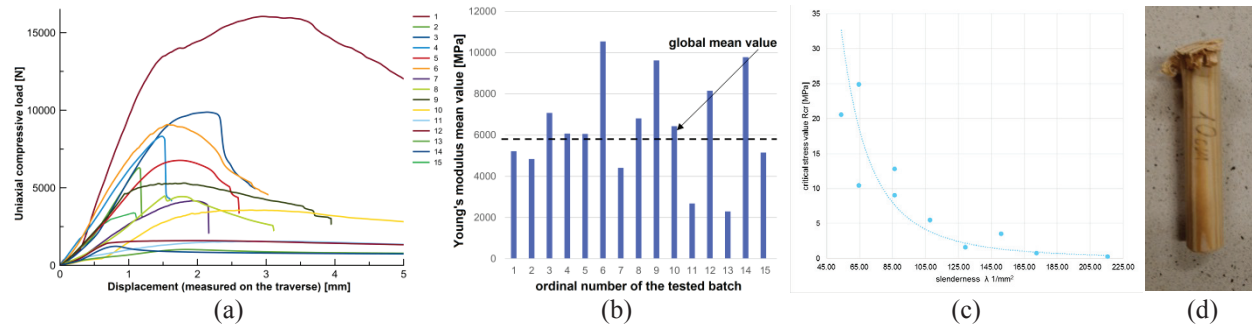


**FIGURE 4.** Results of uniaxial compression test of timber elements: load – displacement diagrams of representative samples for 15 batches used (a), mean value of Young's modulus for every batch (b), the dependence between the slenderness and the critical stress value for samples tested for buckling occurrence (c) and a photo showing failure of sample in the vicinity of support (d)

For each pine timber sample, again, a set of load – displacement diagrams were obtained on the basis of the results provided by the testing machine. A representative sample from each batch was demarcated in Fig. 4a. It is worth noting, that for a widely used material such a scattering of the curves is surprising and undesirable. Some samples were also failing by splitting, their results were deducted from the batch set. The uniaxial test results shown in Fig. 4a were recalculated into a $\sigma/\varepsilon$ relationship, and into respective elastic moduli in MagicPlot, similarly to the plastics tests. The mean values of the modulus for each batch are shown in Fig. 4b, along with a dashed line indicating a global mean value of Young's modulus of pine timber assessed in the experiment. The mean value of Young's modulus was calculated equal to $E_{mean}$ = 5948.913 MPa (a value astonishingly lower – ca. 63% – than the minimal reference value for pine wood in dry air conditions, equal to $E_{PINE}$ = 16000 MPa [5]), the obtained standard deviation of the modulus was equal to $s_E$ = 2055.515 MPa. The following values give a variance coefficient $CoV$ = 0.35, again strongly exceeding the value of 0.05, suggesting the analyzed material is of poor quality.

Furthermore, a test using 15 pine timber samples with various lengths was conducted to assess the minimal length of the sample for which the buckling was observed, resulting in a demarcation value of 200 mm. In Fig. 4c the dependence between the slenderness and the critical stress value was shown, and an Eulerian hyperbola was approximated. Again, only the results from buckled samples were taken into account. Additionally, the most commonly occurring failure mechanism of stocky samples (splitting of the ends) is shown in Fig. 4d. It is generated by friction forces between the sample and the pressing surfaces. However, due to the chosen link type of the elements in the real–life structure and the fact that the ends of the wooden cylinders were drilled to install the coupler can lead to this kind of failure mechanism, so results from tests of these samples were treated as plausible.

## Tensioned elements' experimental tests

All nylon monofilament tendons had a full circular cross–section of $d$ = 1.5 mm and a set length of $L$ = 30.0 cm. However, only 5 batches (out of 20 batches analyzed) were tested as directly supported in the clamps of the testing machine, whereas the latter 15 batches were equipped with an indirect support constructed on a snap hook, the link between the sample and the support hook was formed as a fisherman's bend knot.

For steel tendons experimental analysis, the 6×7(6/1) single layer fiber core stainless steel wire ropes of $d_{tot}$ = 2.0 cm were chosen. Similar to nylon tests, 5 batches of cables were analyzed as directly supported in the clamps of the testing machine, 15 batches were tested with an indirect support conditions. For these indirectly supported elements, every sample had two loops on its ends, the thimble–based loops were either clamp–griped (5 batches) or ferruled (10 batches). The clamp–griped batches and a half of the ferruled batches were put directly into the clamps (the clamps did not press the loops, but transmitted the load through a rigid member), the latter 5 ferruled batches were additionally linked with a snap hook, and the hook was inserted in the clamps of the machine.

The tendon members were at first subjected to a static tensile test. For minimizing the initial slip of the elements, the elements were pre–loaded with a 25 N starting force. The force was again applied by a traverse in a displacement control approach, the test was carried out with a constant speed of 25 mm/min.

The test stands for tensioned specimen is shown in Fig. 5a and Fig 5b.



(a)                    (b)

**FIGURE 5.** The test stand for tensile tests, where the tendons were installed in the clamps indirectly, through a snap hook – the nylon monofilament tendon is attached to the hook using a fisherman's bend knot (a) and the steel wire is clamp–griped (b)
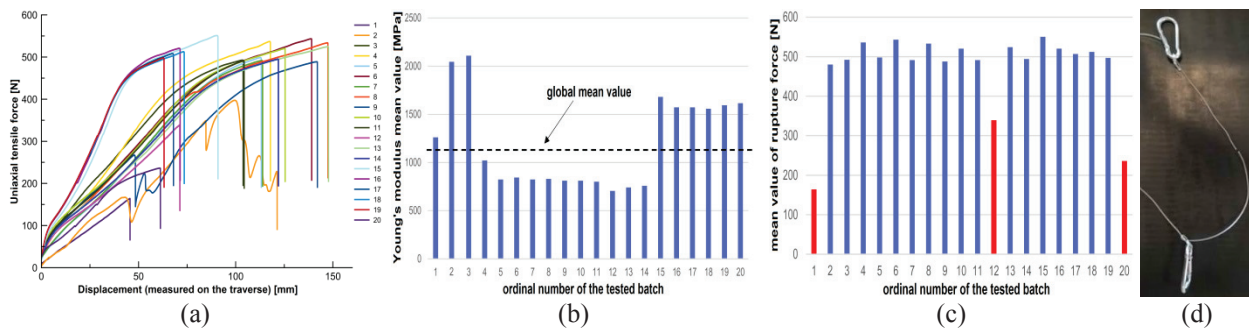


(a)                    (b)                    (c)                    (d)

**FIGURE 6.** Results of uniaxial tension test of nylon tendons: load – displacement diagrams of representative samples for 20 batches used (a), mean values of Young's modulus for every batch (b), the mean value of rupture force for every batch (c) and a photo depicting rupture failure of a sample in its middle (d)

First of all, for every nylon monofilament sample, load – displacement diagrams were obtained on the basis of the results provided by the testing machine. A representative sample from each batch was depicted in Fig. 6a. The tensile test results shown in Fig. 6a were then recalculated into a $\sigma/\varepsilon$ relationship, and further – into respective elastic moduli in MagicPlot. The mean values of the modulus for each batch are shown in Fig. 6b, along with a dashed line indicating a global mean value of Young's modulus of PA6/PP/PET monofilament, assessed on the basis of the experiment. It may be observed, that the results are very bipolar – half of the batches indicate a modulus equal to ca. 750 MPa, whereas the other half provide significantly higher moduli, resulting in a total mean value of $E_{mean} = 1154.632$ MPa. This is a satisfying value, taking into account the reference values for PA6/PP/PET monofilament equal to $E_{NYLON} = (900 - 1550)$ MPa [6]. The obtained standard deviation of the modulus was equal to $s_E = 425.925$ MPa, which gives a variance coefficient $CoV = 0.37$, again strongly exceeding the value of 0.05, acceptable for structural materials' tests [6]. This is surely caused by the above mentioned bipolar moduli values provided by different batches.

Furthermore, a plastic rupture force was assessed, for every batch mentioned above. The results of the tests are given in Fig. 6c. It should be pointed out, that for three batches (no 1, 12, and 20) the force was significantly smaller. The assessed global mean value, equal to $N_{rupt} = 512.3$ N is calculated omitting these batches – because of visible imperfections of the samples introduced by an incorrect storage of the material by the supplier, the rupture force capacity was clearly influenced.

In Fig. 6d, a failed sample is depicted. Please note, that the rupture occurred in the middle of the sample, rather than in the vicinity of the knot. This means, that the tangling of the knot does not introduce imperfections to the sample, the knot is tangled strongly and does not induce slipping of the sample on the snap hooks. Some of the samples from batches no 1, 12 and 20 failed near the knot, which confirms the statement given previously.
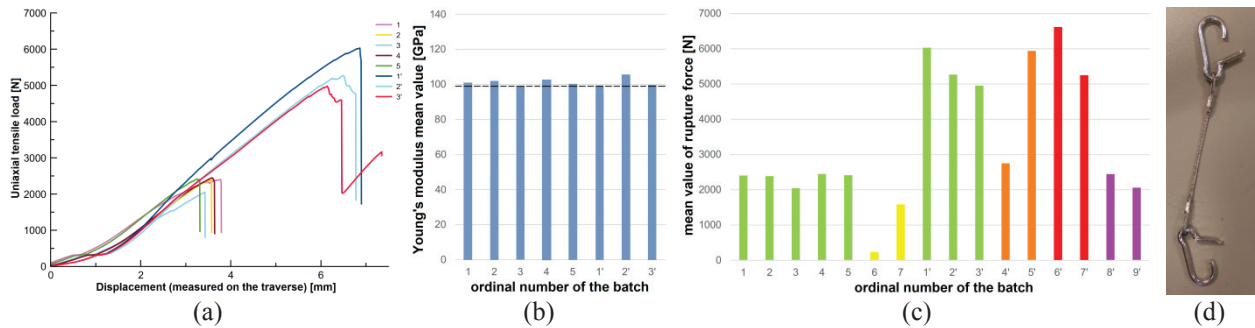
**FIGURE 7.** Results of uniaxial tension test of steel wires: load – displacement diagrams of representative samples for 8 selected batches used (a), mean values of Young's modulus for selected batches (b), the mean value of rupture force for selected batches (c) and a photo depicting an undesirable plastic failure of a snap hook (d)

Only 8 batches are chosen to be presented – 5 batches with a direct clamping in the machine are chosen to be presented (no 1 – 5), along with 3 batches clamped indirectly, without snap hook, ferruled (no 1' – 3', the solution of the tendon finally adopted). For those batches, the load – displacement diagrams for steel 6×7(6/1) single layer fibre core wire ropes were obtained on the basis of the results provided by the testing machine. A representative sample from each batch was depicted in Fig. 7a. Afterwards, the tensile test results shown in Fig. 7a were recalculated into a $\sigma/\varepsilon$ relationship, and further – into respective elastic moduli in MagicPlot. The mean values of the modulus for batches under consideration are shown in Fig. 7b, along with a dashed line indicating a global mean value of Young's modulus. The assessed mean value of the Young's modulus for steel wires was equal to $E_{mean}$ = 98256.601 MPa, which is a satisfying value, taking into account the reference value for the wires given by the manufacturer as equal to $E_{WIRE}$ = 95000 MPa (a satisfying, ca. 3% discrepancy to the reference value). The obtained standard deviation of the modulus was equal to $s_E$ = 7548.976 MPa, which gives a variance coefficient $CoV$ = 0.08, exceeding the value of 0.05 only slightly, therefore almost acceptable.

A plastic rupture force was also assessed in this experiment, the results of the tests are given in Fig. 7c. Not only are the results given for the batches mentioned above (indicated in green), but also two representative rupture forces for other types of clamping are shown – batches 6 and 7 (yellow) were clamp–griped on a snap hook by hand, batches 8' and 9' (purple) were clamp–griped on a snap hook using a wrench, batches 4' and 5' (orange) were ferruled on a snap hook by hand and batches 6' and 7' (red) were ferruled on a snap hook by a crimp. The assessed global mean value from 8 key batches was equal to $N_{rupt}$ = 5419.1 N.

In Fig. 7d, a peculiarly failed sample is depicted. Please note, that the failure took place not in the wire, but in the snap hook, the weakest link in the system (plasticization of the hook). Although, adopting snap hooks of better quality in the subsequent experiments proved to be helpful, it was decided to discard these elements in further use.

# NUMERICAL STUDY OF THE GEOMETRY – SENSITIVITY ANALYSIS AND NUMERICAL OPTIMIZATION

Basing on the experimental results of elastic moduli of used materials, supported with manufacturers' designations of non–assessed parameters, both variants of the structure were also analyzed in the SOFiSTiK commercial FEM software [7]. The support ring was modelled with 12–dof beam elements, whereas the bars were modelled as 6–dof truss elements and the tendons as 6–dof cable elements.

Plastics – nylon tendons and PVC–U pipes were described by bilinear elastic–plastic material law, predefined in SOFiSTiK software, the parameters of their material model were derived from aforementioned experimental tests. For standard construction materials – pine timber cylinders and steel wires, a standard linear elastic–plastic model was proposed with standardized parameters (omitting the experimentally derived elastic moduli).

Dead load, climatic loads (wind and temperature action) and impulse excitation were taken into account. Geometrically and materially nonlinear analysis was conducted, in accordance with TH3 theory, an approach already implemented in SOFiSTiK. Additionally, verification of the FEM model was performed to check if the bars were only axially compressed and the tendons axially elongated in every step of the nonlinear numerical analysis.

To ensure the possibility of carrying out numerical calculations, the truss elements had to be supported on spring elements of an infinitesimal elasticity coefficient, hence the support forces of the elements are also infinitely small,

consistent with real conditions. The wooden frame was modelled as simply supported, all joints between the frame, bars and tendons were assumed as hinged.

The visualization of the Fuller dome FEM model in SOFiSTiK software is shown in Fig. 8. Please note, that for the sake of clarity of the figure, the support frame was replaced with nodal supports.
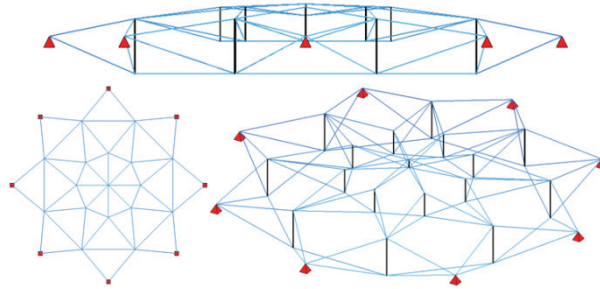


**FIGURE 8.** The visualization of the pre – optimized Fuller's dome FE model, generated in SOFiSTiK Animator module

## Sensitivity analysis of the Fuller's dome

Prior to the target optimization process, a sensitivity analysis of the initial construction of the Fuller system tensegrity dome has been carried out. The analysis was planned to identify the design variables decisive for the tensegrity system structural response. Primarily, the impact of variations of these parameters on the distribution of internal forces has been taken into account, secondly their impact on the vertical displacements was also investigated. The latter was taken as the target function for the optimization.

Sensitivity analysis was performed categorizing the variables in three different groups. Group "A" incorporated the variation of cross sectional diameter for both types of elements, the variables for the elastic moduli change and the cable elements prestressing force detention – the random multiplier for this group was taken from an uniform distribution with border values of 0.50 and 1.50. Group "B" incorporated the length diversity of the elements and the dome nodes elevation imperfections, its random multiplier also was an uniform distribution with border values of 0.50 and 1.50. Finally, group "C" consisted of the variables representing and change in the relations between radii forming the structure, its random multiplier also was an uniform distribution with border values of 0.133 and 0.533 (0.333 being the initial value – all radii were the same).

Sensitivity analysis results for the vertical displacement of the central node of the dome [mm] versus the change for five discrete realizations of five chosen variables (the change in [%]) is shown in Fig. 9.
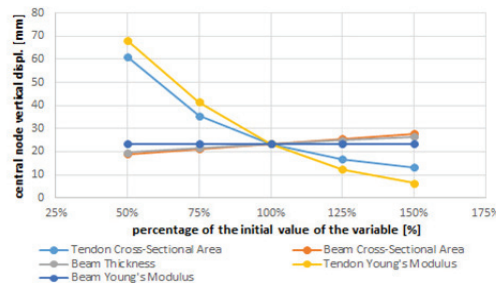


**FIGURE 9.** Sensitivity analysis for the vertical displacement of dome's central node versus the change in five chosen variables

## Simulation – based parametric optimization of the Fuller's dome numerical model

On the basis of sensitivity analysis it was decided, that the variables chosen as key parameters for the desired structural response values will come from groups "B" and "C".

Three values of lower ordinates of the bars in each of the rings of the dome (synonymous with lengths of compressed wooden bars) were chosen as first three variables ($x_1$, $x_2$, $x_3$) – variable *WYS1* is connected to the outer (larger) ring of bars, variable *WYS2* is connected to the inner (smaller) ring of bars, whereas variable RZ1 represents the change of lower ordinate of the key element of the dome (generates the height of the central bar).

Please note, that the discussed variables change the bars in the ring the same way (every length of bar element in one ring has the same set value). Please also take into account that the upper ordinates of the above mentioned bar elements remain unchanged in the optimization process, according to the initial assumption of a fixed arc shape.

Also, two distances between bars along the radial dimension (synonymous with lengths of tensioned steel wires) were chosen as last two variables ($x_4$, $x_5$) – variable $R1$ denotes the smaller ring radius and variable $R2$ denotes the larger ring radius (both values measured from the center of the dome).

The variables were adopted as uniformly distributed (consisted to the design methodology), with the boundary values (optimization restriction values) taken according to Fig. 10a. For illustrative purposes, two extreme geometries of the dome are presented in Fig. 10b – a minimal (generated taking the minimal values of each final variable) and a maximal (generated taking the maximal values of each final variable) one, supplemented with a mean–value geometry (identical with the initial geometry, given in Fig. 8).

In the FE model generated in SOFiSTiK, the elements of the geometry of random dimensions were parameterized in such a way that a change in the value of a single variable regenerated the whole geometry automatically (a cylindrical coordinate system was used, due to the axial symmetry of the structure).
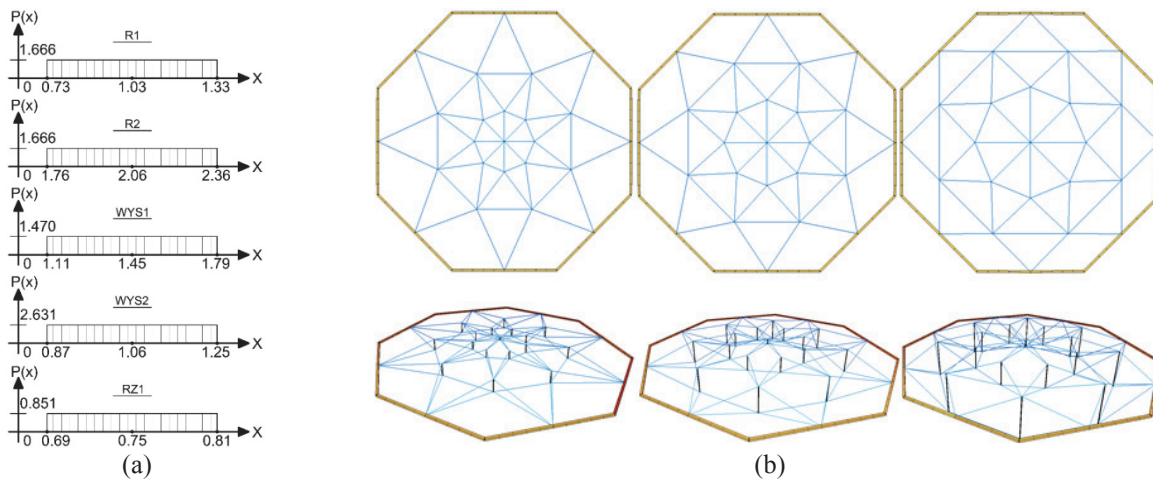


**FIGURE 10.** The final set of random variables taken into account in the optimization process, their boundary values given (a) and visualization of three Fuller's dome FE models (minimal, mean and maximal), generated in SOFiSTiK Animator module

To discern the optimal geometry, the crude Monte Carlo simulation methodology was employed, incorporating the directional sampling variance reduction technique [8]. A number of 1000 calculations of Fuller dome numerical model was performed in SOFiSTiK software, using automated procedures available in RELY module [7]. Conducting the computational process has proven to be a complicated task, as a strong correlation between the variables was observed (for example, the length of the beams acts strongly on the required prestressing of the adjacent cables). Moreover, the various limitations associated with the structure had to be checked in every step of the standard computation algorithm, thus making the computations more time-consuming, similar to numerical experiments conducted in [9].
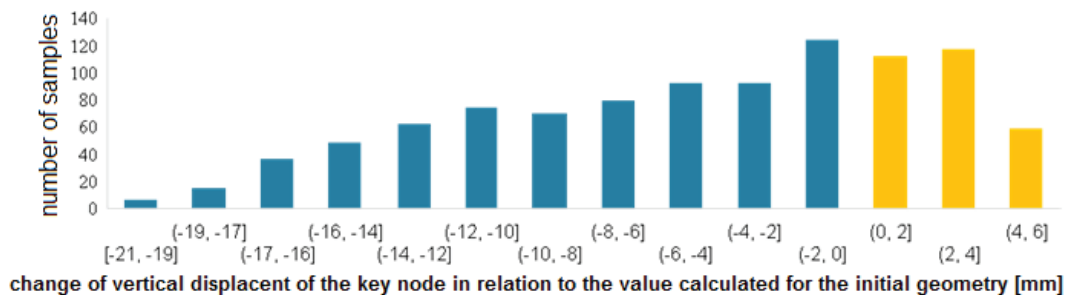


**FIGURE 11.** The histogram of change of maximal vertical displacement of the dome's top node in relation to the value of the displacement calculated for the initial geometry ($U_{max}$ = 36.0 mm)

On the basis of the generated set of samples, an optimized geometry was discerned as the MC methodology sample which generated the lowest value of the result index, defined as the product of dead weight and extreme displacement. The lowest value of the index, equal to 1.2714 kN·mm, was obtained for a structure of a 0.04128 kN dead weight (excluding the timber frame), which in turn gave a maximum displacement of 30.8 mm.

This was achieved for the geometry with the following values of design variables: $R1$ = 1.014 m, $R2$ = 2.056 m, $WYS1$ = 1.481 m, $WYS2$ = 1.071 m and for $RZ1$ = 0.751 m.

Making use of the SOFiSTiK software RELY module [8], comprising the Strurel COMREL package, the probability of structural failure due to the SLS requirements exceeding was calculated using both SORM and Monte Carlo – based Subset Simulation, in a wide variety of geometrical configurations. The optimal dome was deemed to meet the required conditions under the predicted loading in 100%. However, it should be pointed out, that for such structures (tensegrity domes, domes in general), the SLS requirements are far more strict than the ULS ones and they may lead to over – dimensioning of the structure.

## REAL-LIFE STRUCTURE VERIFICATION OF THE EXPERIMENTAL AND NUMERICAL RESULTS

First of all, please note, that the initial Geiger's dome served only as an ascertainment, that such a structure will be safe and erectable, moreover it affirmed that the undertaken technological solutions were proper and sufficient.

Finally, an attempt was made to verify the experimental values and the numerical model results compared with the measurements of an actual design. Series of experiments and measurements were conducted on the erected Fuller structure – the strains, displacements and eigenmodes were surveyed, under the basic load cases induced.

The erected structure is presented in Fig. 12.



**FIGURE 12.** The erected real–life Fuller's dome structure

The differences between the geometry of the optimal model and the geometry of the real model were satisfactory small, with the maximum percentage difference of 6.09% (taking into account that the structure is made of a huge number of separately prepared components). The average geometrical imperfection was only 2.62%.

The structure had a satisfactory damping. For a load case of a 10 cm kinematic extortion, the numerical results were different from the real–life response by only 4.84%. For a testing nodal load case of 0.01 kN, the discrepancy between the model and the real–life structure was negligently small (0.36%).

What is worth noting, during the assembly of the real–life model, one of the elements of the wooden octagonal support frame was damaged during the prestressing of steel tendons. In turn, a separate additional numerical simulation of failure of this element was performed. As a result, a problem related to the redistribution of internal forces in the whole dome structure as a result of a support component damage was additionally solved. The discrepancies between the internal forces of the model and the real–life structure were also negligently small (0.47%). Moreover, it was shown that the structure continued to transfer the dead weight load and no cascade failure was induced. Of course, the SLS requirement had to be discarded in this analysis.

## SUMMARY AND CONCLUSIONS

Numerous technological problems have been encountered during the research. The most important one was to find an appropriate way of clamping of the samples in the testing machine. The tensioned samples must be clamped in a manner that the rupture force value is determinative and the compressed slender samples had to be pressurized in an ideal vertical position, while maintaining a simple support hinged conditions.

Plastics proved to be a very challenging material. It was hard to prepare a sample of a required length, as it was very difficult to tie the knot properly. Moreover, the slip in the knot (when using snap hooks) or tendon slipping on thimbles are non-negligible. If this situation occurs, the inaccuracy of measurement could not be estimated properly.

Mounting samples on snap hooks made them unintentionally eccentric. The best solution was to put the samples in the clamps of the testing machine by their hooks, fully ferruled in a crimp. It was shown, that the samples must be tested with real-life nodes constructed: either the snap hooks attachment or the wire thimbles existence may cause the sample failure in the vicinity of the anchorage.

The experimentally – derived solution of linking elements (the bars had hooks installed on its end, the loops of the wires were put on the hooks, wooden pegs were placed in the hooks to prevent the tendons from falling off during the assembly) fulfilled its purpose in the real – life structure completely.

It was shown, that the stability loss of the bars is a major threat, especially for materials with a low elastic moduli. On the other hand, plastic tendon failure is almost impossible in small tensegrity models. Detangling of the wires may occur much faster than their plastic failure

As for the parametric analysis, it has shown that the dominant design variables for the tensegral domes were the lengths of the compressed elements and the dimensioning of the rings' radii.

Strong nonlinearity of the response surface of the structure was indicated during the simulation – based optimization, hence the following nonlinearity of the limit state function (LSF) is a considerable problem, causing the computations to be complex and very time-consuming and the outcome results may be hard to analyze.

The optimal real–life structure built on the basis of the optimization process proved to work in accordance with the results obtained using FEM.

It is advisable to design and perform experimental tests of the material for the dome's coverage, and to perform the FEM structural analysis considering the wind load effects on the applied shell structure.

## REFERENCES

1.  L. Małyszko, "Static response of axially loaded tensegrity prism. Example of using proprietary programming language" in Lightweight Structures in Civil Engineering – LSCE 2016. Contemporary Problems, edited by J. B. Obrębski (University of Warmia and Mazury Publishing Office, Olsztyn, 2016), pp. 43–48.
2.  W. Ryżyński and J. K. Szlendak, Nowoczesne Hale **16**, 10–14 (2011).
3.  W. Ryżyński and J. K. Szlendak, Nowoczesne Hale **17**, 41–45 (2011).
4.  Ł. Smakosz and I. Kreja, "Experimental and numerical evaluation of mechanical behaviour of composite structural insulated wall panels under edgewise compression" in Advances in Mechanics: Theoretical, Computational and Interdisciplinary Issues, edited by M. Kleiber, T. Burczynski, K. Wilde, et al. (WIB Printing House, Gdańsk, 2016), pp. 521–524.
5.  D. Ferreira, E. Fonseca, C. Pinto and P. Borges, "Tensile strength of pine and ash woods – experimental and numerical study" in M2D2015: Proceedings of the 6th International Conference on Mechanics and Materials in Design, edited by J. F. S. Gomes and S. A. Meguid (INEGI-FEUP, Porto, 2015), pp. 2341–2348.
6.  E. R. Parker, *Materials data book for engineers and scientists* (McGraw-Hill, Michigan, 1967).
7.  J. Górski, M. Oziębło and K. Winkelmann, "Sensitivity analysis of simple random beam models by means of Monte Carlo methods using variance reduction techniques" in Lightweight Structures in Civil Engineering – Contemporary Problems, Proceedings of the 19th LSCE Seminar, edited by J. B. Obrębski and L. Małyszko (Micro-Publisher C-P, Olsztyn, 2013), pp. 42–47.
8.  SOFiSTiK FEA 2016 for Windows. Software Manuals: Animator, ASE, RELY. SOFiSTiK AG, Oberschleissheim, 2017.
9.  U. Radoń, Archives of Civil and Mechanical Engineering **3**, 723–726 (2011).